

RAREFACTION EFFECTS ON SHOCK-WAVE STRUCTURE OF HYPERSONIC FLOW OVER POWER-LAW LEADING EDGES

Wilson F. N. Santos

Combustion and Propulsion Laboratory
National Institute for Space Research
12630-000 Cachoeira Paulista, SP, Brazil
wilson@lcp.inpe.br

Abstract. *This work deals with a numerical study of power-law leading edges situated in a hypersonic flow. The primary aim of this paper is to examine the effect of rarefaction on the shock-wave structure. The rarefaction effect on the shock wave has been investigated by employing the Direct Simulation Monte Carlo (DSMC) method. The work is motivated by interest in investigating power-law shaped leading edges as possible candidates for blunting geometry of hypersonic leading edges. The sensitivity of shock standoff distance, shock thickness and shock wave shape to variations on rarefaction are simulated for altitudes of 70, 80 and 85 km. The analysis shows significant differences on the shock wave structure due to variations not only on the altitude but also on the leading-shape defined by the power-law exponent. It was found that the shock standoff and the shock thickness increased with increasing the altitude.*

Keywords. *DSMC, hypersonic flow, rarefied flow, power-law shape, shock standoff distance, shock wave thickness.*

1. Introduction

Hypersonic waveriders are advanced hypersonic lifting bodies which generate the highest known lift-to-drag (L/D) ratio at high Mach number. A waverider (Nonweiler, 1959) is designed from an inverse process which involves the initial selection of a shock wave and a known analytic flowfield, such as flow over a two-dimensional wedge or flow around a slender cone, followed by the determination of a vehicle geometry which corresponds to the desired flowfield. The potential of generating high lift is obtained by using the attached shock wave as a barrier in order to prevent air flow from the high pressure windward side to the low leeward side. In principle, there is no leakage of high pressure from the bottom surface around the leading edge to the top surface. Nevertheless, in practice, waveriders tend to suffer from viscous effects. As a result, the full potential of waveriders has never been fulfilled, as viscous forces tend to displace the shock wave, and the displacement effect has some influence on the L/D performance.

The successful design of high-lift, low-drag hypersonic configurations will depend on the ability to incorporate relatively sharp-leading edges that combine good aerodynamic properties with acceptable heating rates. However, for practical applications, these sharp leading edges must be blunted for heat transfer, manufacturing, and handling concerns, with associated departures from ideal performance. Typically, a round leading edge with constant radius of curvature (circular cylinder) near the stagnation point has been chosen. Nevertheless, shock detachment distance on a cylinder, with associated leakage, scales with the radius of curvature. Certain classes of non-circular shapes may provide the required bluntness with smaller shock separation than round leading edges, thus allowing manufacturing, and ultimately heating control, with reduced aerodynamic losses.

In this scenario, power-law shaped leading edges ($y \propto x^n$, $0 < n < 1$) may provide the required bluntness for heat transfer, manufacturing and handling concerns with reduced departures from ideal aerodynamic performance. This concept is based on work available in the literature that pointed out, based on Newtonian flow analysis, that these shapes exhibit both blunt and sharp aerodynamic properties.

Numerous studies have been done with the power-law form representing blunt geometries. For the purpose of this introduction, it will be sufficient to describe only a few of these works. The major interest in these works had gone into finding solutions to the hypersonic small disturbance form of the inviscid adiabatic-flow equations. The equations of motion for hypersonic flow over slender bodies can be reduced to simpler form by incorporating the hypersonic slender-body approximations (Van Dyke, 1954). The reduced equations are valid provided $\tau^2 \ll 1$ and $(M_\infty \tau)^{-2}$ is not near one, where M_∞ is the freestream Mach number and τ is a characteristic shock slope. Lees and Kubota (1957) observed that similarity exists for hypersonic flows whenever the shock shape follows a power-law variation with the streamwise distance, provided the hypersonic slender body equations are considered in the limit as $(M_\infty \tau)^{-2} \rightarrow 0$. According to their work, energy considerations combined with a detailed study of the equations of motion show that flow similarity is possible for a class of bodies of the form x^n , provided that $2/3 < n < 1$ for a two dimensional body and $1/2 < n < 1$ for an axisymmetric body. The similarity solutions referred herein are solutions for self-similar flows, i.e., flows in which the flowfield between the shock wave and the body can be expressed in terms of functions which, in suitable coordinates, are independent of one of the coordinate directions.

Mason and Lee (1994) pointed that, for certain exponents, power law shapes exhibit aerodynamic properties similar to geometrically sharp shapes. They suggested the possibility of a difference between shapes that are geometrically

sharp and shapes that behave aerodynamically as if they were sharp. They showed that for values of $0 < n < 1/2$, the leading-edge radius of curvature goes to infinite at the nose, a characteristic of a blunt shape. For values of $1/2 < n < 1$ the leading-edge radius of curvature approaches zero at the nose, a characteristic of a sharp shape. Furthermore, for $2/3 < n < 1$, their computational investigation predicts that the derivative of the pressure coefficient with respect to the body coordinate dC_p/ds approaches $-\infty$ at $x = 0$, a characteristic of a sharp body. In this way, there is a class of body shapes given by $1/2 < n < 2/3$, for which the leading edge may behave aerodynamically like a blunt body, even though the leading-edge radius of curvature is zero, and another one given by $2/3 < n < 1$ for which the leading edge may behave like aerodynamically sharp body even though the leading edge bluntness is infinite. Their analysis describes the details of the geometry and aerodynamics of low-drag axisymmetric bodies by using Newtonian theory. Nonetheless, one of the important aspects of the problem, stagnation point heat transfer, was not considered.

Based on recent interest in hypersonic waveriders for high-altitude/low-density applications, Santos and Lewis (2002) have investigated the sensitivity of the pressure gradient and the stagnation point heating to shape variations of power-law leading edges by considering two-dimensional rarefied hypersonic flow. Through the use of the DSMC method, they showed that the pressure gradient on the power-law shapes is in surprising agreement with that obtained by Mason and Lee (1994) by employing Newtonian Analysis. They also found that the stagnation point heating scales inversely with the square root of the curvature radius for power-law bodies with finite radius of curvature.

Santos and Lewis (2005a) compared power-law shapes to a corresponding circular cylinder in order to determine which geometry would be better suited as a blunting profile. Their analysis also showed that power-law shapes provided smaller total drag than circular cylinder, typically used in blunting sharp leading edges for heat transfer considerations. However, circular cylinder provided smaller stagnation point heating than power-law shapes under the range of conditions investigated. The power-law exponent effect on shock-wave was examined by Santos and Lewis (2005b).

In an effort to obtain further insight into the nature of the shock-wave structure on power-law leading edges under hypersonic transitional flow conditions, a parametric study is performed on these leading edges with a great deal of emphasis placed on the rarefaction effects. In this connection, the primary goal of the present account is to assess the sensitivity of the shock standoff distance, shock wave thickness and shock wave shape to variations not only on the rarefaction experienced by the leading edges but also on the shape of the leading edges via power-law exponent.

For the high altitude/high Knudsen number of interest ($Kn > 0.1$), the flowfield is sufficiently rarefied that continuum method becomes inappropriate. Alternatively, the DSMC method is used in the current study to calculate the rarefied hypersonic two-dimensional flow on the leading edge shapes.

2. Leading Edge Geometry Definition

In dimensional form, the body power-law shapes (Santos and Lewis, 2002) are given by the following expression,

$$y = ax^n \tag{1}$$

where n is the power-law exponent and a is the power-law constant which is a function of n .

The power-law shapes are modeled by assuming a sharp leading edge of half angle θ with a circular cylinder of radius R inscribed tangent to this wedge. The power-law shapes, inscribed between the wedge and the cylinder, are also tangent to them at the same common point where they have the same slope angle. The circular cylinder diameter provides a reference for the amount of blunting desired on the leading edges. It was assumed a leading edge half angle of 10 degrees, a circular cylinder diameter of 10^{-2} m and power-law exponents of $1/2$, $2/3$, and $3/4$. Figure (1a) illustrates schematically this construction for the set of power-law leading edges investigated.

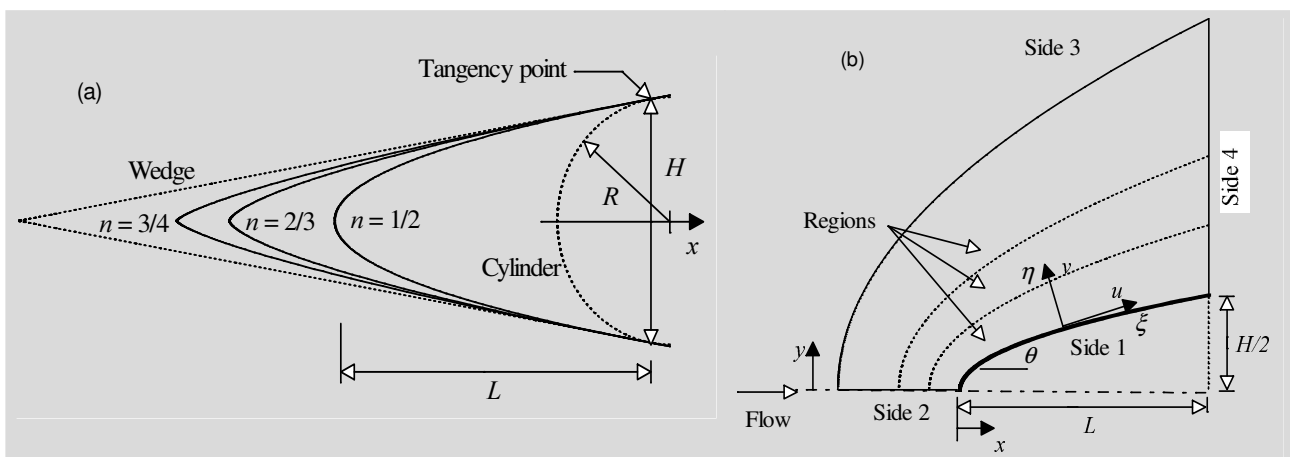


Figure 1: Drawing illustrating (a) the leading edge shapes and (b) the computational domain.

From geometric considerations, the power-law constant a is obtained by matching slope on the wedge, circular cylinder and power-law body at the tangency point. The common body height H at the tangency point is equal to $2R\cos\theta$, and the body length L from the nose to the tangency point in the axis of symmetry is given by $nH/2\tan\theta$. It was assumed that the power-law leading edges are infinitely long but only the length L is considered since the wake region behind the power-law bodies is not of interest in this investigation.

3. Computational Method

The DSMC method (Bird, 1994) has proved to be an extremely useful and flexible tool in the analysis of rarefied hypersonic non-equilibrium gas flows. In this study, the particle simulations were performed by using the DSMC method developed by Bird (1994). The DSMC method simulates fluid flow by using thousands to millions of particles. These particles are tracked as they move, collide and undergo boundary interactions in simulated physical space. In addition, particle motions are assumed to be decoupled from particle collisions and each process is computed independently during a time step used to advance the simulation. This time step must be sufficiently small in comparison with the local mean collision time (Garcia and Wagner, 2000, and Hadjiconstantinou, 2000) such that the assumption of decoupled particle motions and collisions is not violated.

The reliability of the method is entirely dependent on the accuracy of the collision models used to simulate particles interactions. The molecular collisions are modeled using the variable hard sphere (VHS) molecular model (Bird, 1981) and the no time counter (NTC) collision sampling technique (Bird, 1989). The VHS model employs the simple hard sphere angular scattering law so that all directions are equally possible for post-collision velocity in the center-of-mass frame of reference. However, the collision cross section is a function of the relative energy in the collision. The energy exchange between kinetic and internal modes is controlled by the Borgnakke-Larsen statistical model (Borgnakke and Larsen, 1975). Simulations are performed using a non-reacting gas model consisting of two chemical species, N_2 and O_2 . Energy exchanges between the translational and internal modes are considered. For this study, the relaxation numbers of 5 and 50 were used for the rotation and vibration, respectively.

4. Computational Flow Domain and Grid

The computational domain is made large enough so that the upstream and side boundaries can be specified as freestream conditions. Figure 1(b) depicts the physical extent of the computational domain for the present simulations. Advantage of the flow symmetry is taken into account, and molecular simulation is applied to one-half of a full configuration. The computational domain is divided into an arbitrary number of regions, which are subdivided into computational cells. The cells are further subdivided into four subcells, two subcells/cell in each coordinate direction. The linear dimensions of the cells should be small in comparison with the scale length of the macroscopic flow gradients normal to the streamwise directions, which means that the cell dimensions should be of the order of or even smaller than the local mean free path (Alexander et al., 1998 and 2000). In the current DSMC code, the cell provides a convenient reference for the sampling of the macroscopic gas properties, while the collision partners are selected from the same subcell. As a result, the flow resolution is much higher than the cell resolution.

Referring to Fig. (1b), side 1 is defined by the body surface. Diffuse reflection with complete thermal surface accommodation is the condition applied to this side. Side 2 is a plane of symmetry, where all flow gradients normal to the plane are zero. This plane is equivalent to a specular reflecting boundary at the molecular level. Side 3 is the freestream side through which simulated molecules enter and exit. Finally, the flow at the downstream outflow boundary, side 4, is predominantly supersonic and vacuum condition is specified (Guo and Liaw, 2001). At this boundary, simulated molecules can only exit.

Numerical accuracy in DSMC method depends on the grid resolution chosen as well as on the number of particles per computational cell. Both effects were investigated to determine the number of cells and the number of particles required to achieve grid independence solutions. The grid generation scheme used in this study follows that procedure presented by Bird (1994). Along the outer boundary (side 3) and the body surface (side 1) (see Fig. (1b)), point distributions are generated in such way that the number of points on each side is the same (ξ -direction in Fig. (1b)). Then, the cell structure is defined by joining the corresponding points on each side by straight lines and then dividing each of these lines into segments which are joined to form the system of quadrilateral cells (η -direction in Fig. (1b)). The distribution can be controlled by a number of different distribution functions that allow the concentration of points in regions where high flow gradients or small mean free paths are expected.

A grid independence study was made with three different structured meshes in each coordinate direction. The effect of altering the cell size in the ξ -direction was investigated with grids of 35(coarse), 70(standard) and 105(fine) cells, and 50 cells in the η -direction for power-law exponent of 1/2. In analogous fashion, an examination was made in the η -direction with grids of 25(coarse), 50(standard) and 75(fine) cells, and 70 cells in the ξ -direction for power-law exponent of 1/2. Each grid was made up of non-uniform cell spacing in both directions. The effect (not shown) of changing the cell size in both directions on the heat transfer, pressure and skin friction coefficients was rather insensitive to the range of cell spacing considered, indicating that the standard grid, 70x50 cells, for the power-law shape defined by $n = 1/2$ is essentially grid independent. A similar procedure was performed for the two other cases

investigated. Results indicated that a grid of 80x50 and 90x50 for power-law exponents of 2/3 and 3/4 respectively, were considered fully independent. Of particular interest is the number of cells in the η -direction for the three power-law cases investigated. It should be emphasized that, even though the number of cells is the same, the computational domain size is different for each one of the cases; side 2 shown in Fig. (1b) corresponds to $8\lambda_\infty$, $6\lambda_\infty$ and $5\lambda_\infty$ for power-law exponents of 1/2, 2/3 and 3/4, respectively, where λ_∞ is the freestream mean free path.

In a second stage of the grid independence investigation, a similar examination was made for the number of molecules. The standard grid for power-law exponent of 1/2, 70x50 cells, corresponds to, on average, a total of 121,000 molecules. Two new cases using the same grid were investigated. These two new cases correspond to 108,000 and 161,000 molecules in the entire computational domain. As the three cases presented approximately the same results (see Santos and Lewis, 2002) for the heat transfer, pressure and skin friction coefficients, hence the standard grid with a total of 121,000 molecules is considered enough for the computation of the shock wave structure.

5. Freestream and Flow Conditions

Rarefaction effects are investigated for altitudes of 70, 80 and 85 km. For each one of the altitude investigated, the freestream Mach number M_∞ and the wall temperature T_w are kept to the constant values of 12 and 880 K, respectively. Freestream Mach number M_∞ of 12 corresponds to freestream velocity V_∞ of 3.56, 3.236 and 3.236 km/s for altitude of 70, 80 and 85 km, respectively.

Table (1) summarizes the freestream and flow conditions used in the present calculations. The gas properties considered in the simulation are those given by Bird (1994) and tabulated in Tab. (2). Referring to Tabs (1) and (2), T_∞ , p_∞ , ρ_∞ , n_∞ , μ_∞ and λ_∞ stand respectively for temperature, pressure, density, number density, viscosity and mean free path, and X , m , d and ω account respectively for mole fraction, molecular mass, molecular diameter and viscosity index.

Table 1: Freestream Conditions

Altitude (km)	T_∞ (K)	p_∞ (N/m ²)	$\rho_\infty \times 10^5$ (kg/m ³)	$n_\infty \times 10^{-20}$ (m ⁻³)	$\mu_\infty \times 10^5$ (Ns/m ²)	$\lambda_\infty \times 10^3$ (m)	V_∞ (m/s)
70	220.0	5.582	8.753	18.2090	1.455	0.903	3560
80	181.0	1.040	1.999	4.1586	1.253	3.960	3236
85	181.0	0.414	0.796	1.6550	1.253	9.940	3236

Table 2: Gas Properties

	X	m (kg)	d (m)	ω
O ₂	0.237	5.312×10^{-26}	4.01×10^{-10}	0.77
N ₂	0.763	4.65×10^{-26}	4.11×10^{-10}	0.74

The overall Knudsen number Kn_∞ , defined as the ratio of the freestream mean free path λ_∞ to the diameter of the circular cylinder, corresponds to 0.0903, 0.3960 and 0.9940 for altitude of 70, 80 and 85 km, respectively. Finally, the Reynolds number Re_∞ per unit of meter, based on conditions in the undisturbed stream is 21416.3, 5165 and 2055 for altitude of 70, 80 and 85 km, respectively.

6. Computational Procedure

The knowledge of the shock wave displacement is especially important in waverider configurations (Nonweiler, 1959), since these hypersonic configurations usually rely on shock wave attachment at the leading edge to achieve their L/D ratio at high-lift and low drag coefficients. In addition, the ability to predict the shape and location of shock waves is of primary importance in the analysis of aerodynamic interference.

In the present account, the shock wave structure, defined by shape, thickness and detachment of the shock wave, is predicted by employing a procedure based on the physics of the particles. In this scenario, the flow is assumed to consist of three distinct classes of molecules: those molecules from the freestream that have not been affected by the presence of the leading edge are denoted as class I molecules; those molecules that, at some time in their past history, have struck and been reflected from the body surface are denoted as class II molecules; and finally, those molecules that have been indirectly affected by the presence of the body are defined as class III molecules. For illustration purpose, Fig. (2a) displays the definition for the molecular classes adopted in this simulation.

According to Fig. (2a), it is assumed that the class I molecule changes to class III molecule when it collides with class II or class III molecule. Class I or class III molecule is progressively transformed into class II molecule when it interacts with the body surface. Also, a class II molecule remains class II regardless of subsequent collisions and

interactions. Hence, the transition from class I molecules to class III molecules may represent the shock wave, and the transition from class III to class II may define the boundary layer.

A typical distribution of class III molecules along the stagnation streamline for blunt leading edges is displayed in Fig. (2b), together with the definition used to determine the thickness, displacement and shape of the shock wave. In this figure, the distance x along the stagnation streamline is normalized by the radius of the reference circular cylinder (see Fig. (1b)) and f_{III} is the number of molecules for class III to the total amount of molecules inside each cell.

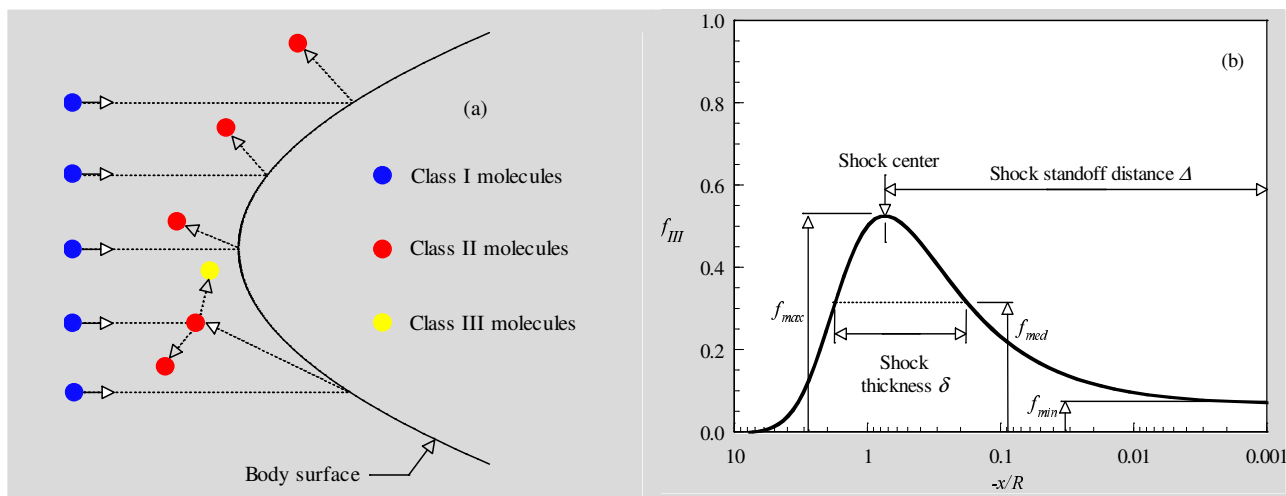


Figure 2: (a) Drawing illustrating the classification of molecules and (b) Schematic of shock wave structure.

In a rarefied flow, the shock wave has a finite region that depends on the transport properties of the gas, and can no longer be considered as a discontinuity obeying the classical Rankine-Hugoniot relations. In this context, the shock standoff distance Δ is defined as being the distance between the shock wave center and the nose of the leading edge along the stagnation streamline. As shown in Fig. (2b), the center of the shock wave is defined by the station that corresponds to the maximum value for f_{III} . The shock wave thickness δ is defined by the distance between the stations that correspond to the mean value for f_{III} . Finally, the shock wave shape (shock wave “location”) is determined by the coordinate points given by the maximum value in the f_{III} distribution along the lines departing from the body surface, i.e., η -direction as shown in Fig. (1b).

7. Computational Results and Discussion

Having presented the definition for the shock-wave structure, it becomes instructive to focus on the computational results. In this connection, the purpose of this section is to discuss and to compare differences on the shape, thickness and displacement of the shock wave due to variations on rarefaction as well as on the power-law exponent, which defines the leading-edge shape. Before proceeding with the presentation of the shock-wave properties, it is desirable to discuss the results related to the molecular class distribution.

7.1. Molecular Class Distribution

The distribution of molecules for classes I, II and III along the stagnation streamline is displayed in Figs. (3), (4) and (5) for power-law exponent n of 1/2, 2/3 and 3/4, respectively. In this set of plots, f_I , f_{II} and f_{III} are the ratio of the number of molecules for class I, II and III, respectively, to the total amount of molecules inside each cell along the stagnation streamline. Also, the flow is from left to right and the distance x along the stagnation streamline is normalized by the radius R of the reference circular cylinder.

Interesting features are observed in Figs. (3), (4) and (5). Of great significance in these figures is the behavior of the class I molecules for sharp and blunt leading edges. It should be noticed that molecules from freestream, represented by class I molecules, do not reach the nose of the leading edge for that case illustrated in Fig. (3a), which represents a blunt leading edge at an altitude of 70 km. In contrast, class I molecules collide with the nose of the leading edge, even after the establishment of the steady state, for that case shown in Fig. (5a), which represents a sharp leading edge at the same altitude. This is explained by the fact that density increases much more for blunt leading edges in the stagnation region and reaches its maximum value at the stagnation point. In this connection, the buildup of particle density near the nose of the leading edge acts as a shield for the molecules coming from the undisturbed stream.

The buildup of particles density at the vicinity of the stagnation point decreases as the altitude increases from 70 to 85 km. As a result, the class I molecules reach the nose of either blunt or sharp leading edges, as displayed by Figs. (3c), (4c) and (5c). The effect of increasing the altitude is to create a more rarefied situation in which the shock standoff

increases and the shock wave center locates more away from the body, since the Kn_∞ increases. The presence of the body, propagated by random motion of the molecules, is communicated to a larger distance ahead of the body, since the molecules interact little with each other and collisions among them are less frequent.

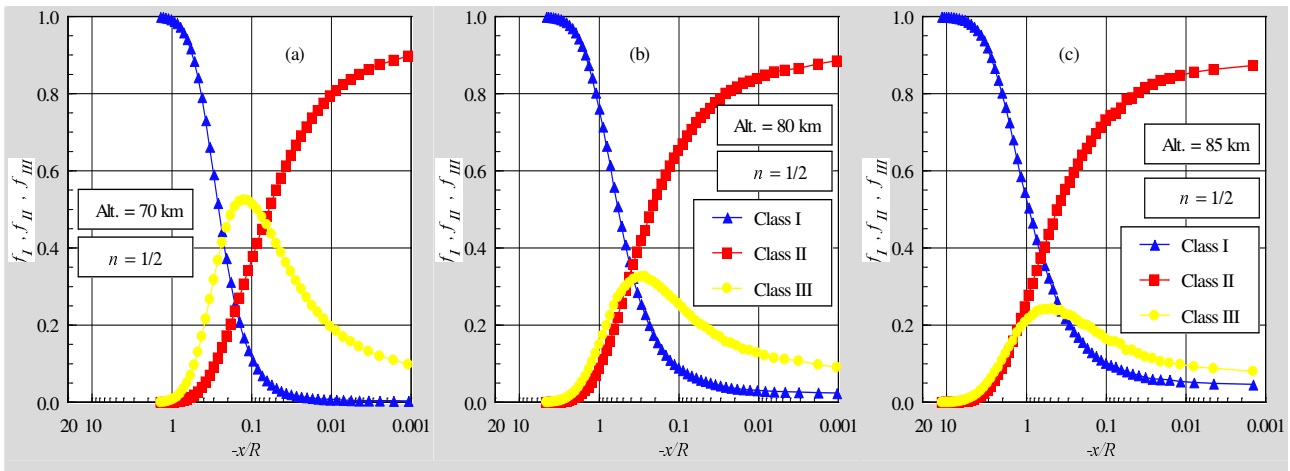


Figure 3: Distributions of molecules for classes I, II and III along the stagnation streamline for power-law exponent n of $1/2$ and altitude of (a) 70, (b) 80 and (c) 85 km.

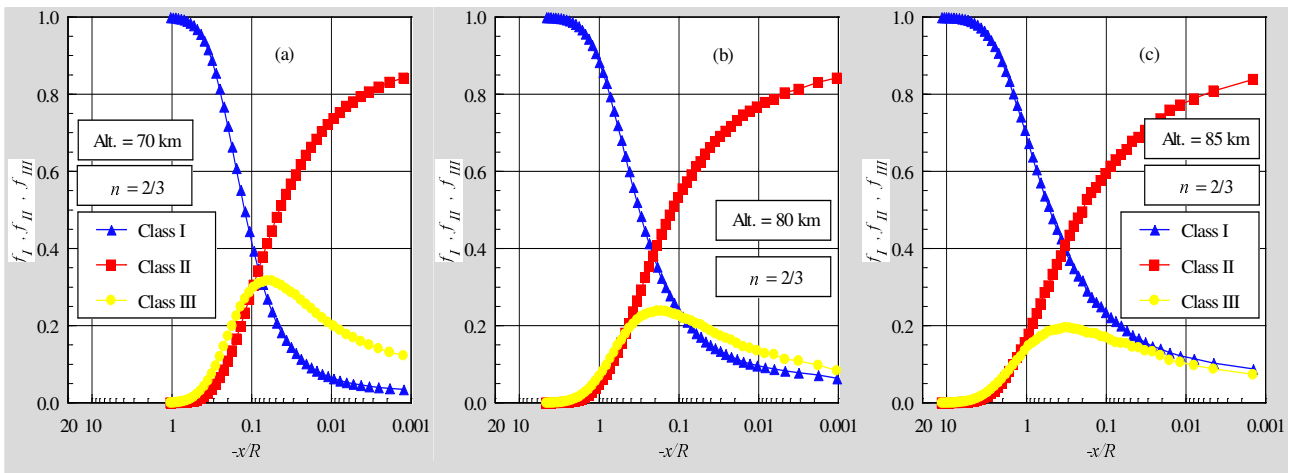


Figure 4: Distributions of molecules for classes I, II and III along the stagnation streamline for power-law exponent n of $2/3$ and altitude of (a) 70, (b) 80 and (c) 85 km.

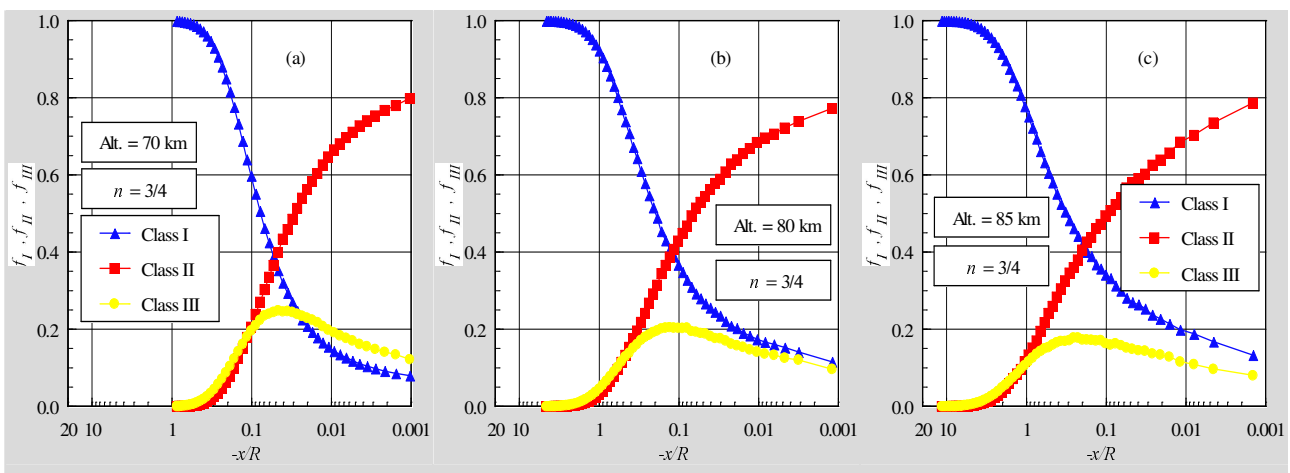


Figure 5: Distributions of molecules for classes I, II and III along the stagnation streamline for power-law exponent n of $3/4$ and altitude of (a) 70, (b) 80 and (c) 85 km.

In this connection, of particular interest in Figs. (3), (4) and (5) is the upstream disturbance of the flowfield. It is clearly seen in this set of figures that the flowfield upstream disturbance increases with increasing the altitude. As an illustrative example, for power-law exponent of 1/2, the class I molecules defined by $f_i = 0.99$ is located at an upstream distance x/R of around 1.0, 3.1 and 6.0 for altitudes of 70, 80 and 85 km, respectively. As a reference, for power-law exponent of 3/4, the class I molecules defined by $f_i = 0.99$ is located at an upstream distance x/R of around 0.5, 2.2 and 5.0 for altitudes of 70, 80 and 85 km, respectively. Therefore, it is observed that the rarefaction effect on the upstream disturbance is less pronounced as the leading edge becomes aerodynamically sharp.

7.2. Shock Wave Standoff Distance

The shock wave standoff distance Δ for the leading edges corresponding to n of 1/2, 2/3 and 3/4 can be observed in Figs. (3) (4) and (5), respectively. It is apparent from these plots that there is a discrete shock standoff distance for the cases shown. In conformity with the definition presented in Fig. (2b), the calculated shock wave standoff distance Δ , normalized by the radius R of the reference circular cylinder, is tabulated in Tab. (3) for the cases investigated. As would be expected, the shock standoff distance increases with increasing the altitude. By increasing the altitude, or increasing in the Knudsen number Kn_∞ , the presence of the leading edge is communicated to a larger distance ahead of the nose of the leading edge since the molecules interact little with each other and collisions among them are less frequent. As a result, the center of the shock wave is located more away from the nose, resulting in a shock standoff rise. Moreover, the shock standoff distance decreases by increasing the power-law exponent n . This is explained by the fact that, as the power-law exponent n increases from 1/2 to 3/4 the leading edge changes from blunt to sharp one. As a result, the leading edge becomes more streamlined, and the presence of the leading edge is communicated to a smaller distance ahead of the leading edge. As a reference, for the $n = 1/2$ case, the shock standoff distance for altitudes of 70, 80 and 85 km is around 2.9, 2.5 and 2.3 times, respectively, larger than those for the $n = 3/4$ case.

Table 3: Dimensionless shock wave standoff distance Δ/R for power-law leading edges.

Altitude (km)	$n = 1/2$	$n = 2/3$	$n = 3/4$
70	0.122	0.062	0.042
80	0.296	0.172	0.119
85	0.525	0.311	0.230

Before proceeding with the analysis, it is desirable to compare the shock standoff distance for power-law shapes with that for the circular cylinder, shown in Fig. (1a). According to Santos and Lewis (2005a), the circular cylinder provides a larger shock standoff distance, i.e., Δ/R of 0.297 for an altitude of 70 km. This value is about 2.4, 4.8 and 7.1 times larger than that for power-law exponent n of 1/2, 2/3 and 3/4, respectively, for the same altitude. The results tend to confirm the expectation that the shock standoff distance for sharp leading edge is smaller than that for blunt leading edge. In fact, the power-law bodies behave as if they had a sharper profile than the representative circular cylinder, as shown in Fig.(1a).

It is important to mention that shock standoff distance becomes important in hypersonic vehicles such as waveriders, which depend on leading edge shock attachment to achieve their high lift-to-drag ratio at high lift coefficient. In this connection, power-law shapes seem to be more appropriate than the circular cylinder, since they present reduced shock wave detachment distances. Nevertheless, smaller shock detachment distance is associated with a higher heat load to the nose of the body. According to Santos and Lewis (2002), the heat transfer coefficient C_{ho} ($= 2q_w/\rho_\infty V_\infty^2$) at the stagnation point for power-law shapes defined by n of 1/2, 2/3 and 3/4, at an altitude of 70 km, is around 1.7, 2.1 and 2.3 times larger than the heat transfer coefficient for the circular cylinder at the same conditions. Consequently, it should be notice from this comparison that the ideal blunting leading edge depends on the context. If shock standoff distance is the primary issue in leading edge design of hypersonic waveriders, then power-law shapes are superior to round leading edges (circular cylinder). In contrast, if the stagnation point heating is the important parameter in the hypersonic vehicle design, then round shapes seem to be superior to the power-law shapes.

7.3. Shock Wave Thickness

The shock wave thickness δ along the stagnation streamline can be obtained from Figs. (3), (4) and (5) for the power-law shapes based on the definition of the shock wave thickness shown in Fig. (2b). As a result of the calculation, Tab. (4) tabulates the shock-wave thickness δ , normalized by the radius R of the reference circular cylinder, for the cases investigated.

The circular cylinder provides a much larger shock thickness, i.e., δ/R , of 0.605 for an altitude of 70 km. Compared to the power-law shapes, this value is about 2.1, 3.8 and 5.2 times larger than that for power-law exponent n of 1/2, 2/3 and 3/4, respectively, for the same altitude.

Table 4: Dimensionless shock wave thickness δ/R for power-law leading edges.

Altitude (km)	$n = 1/2$	$n = 2/3$	$n = 3/4$
70	0.285	0.161	0.117
80	0.732	0.514	0.391
85	1.390	1.034	0.800

7.4. Shock Wave Shape

The shock wave shape, defined by the shock wave center location, is obtained by calculating the position that corresponds to the maximum f for class III molecules in the η -direction along the body surface (see Fig. (1b)). Figures (6a), (6b) and (6c) display the shock-wave shape on power-law bodies defined by n of $1/2$, $2/3$ and $3/4$, respectively, as a function of the altitude. In this set of plots, the Cartesian coordinates x and y are normalized by the radius R .

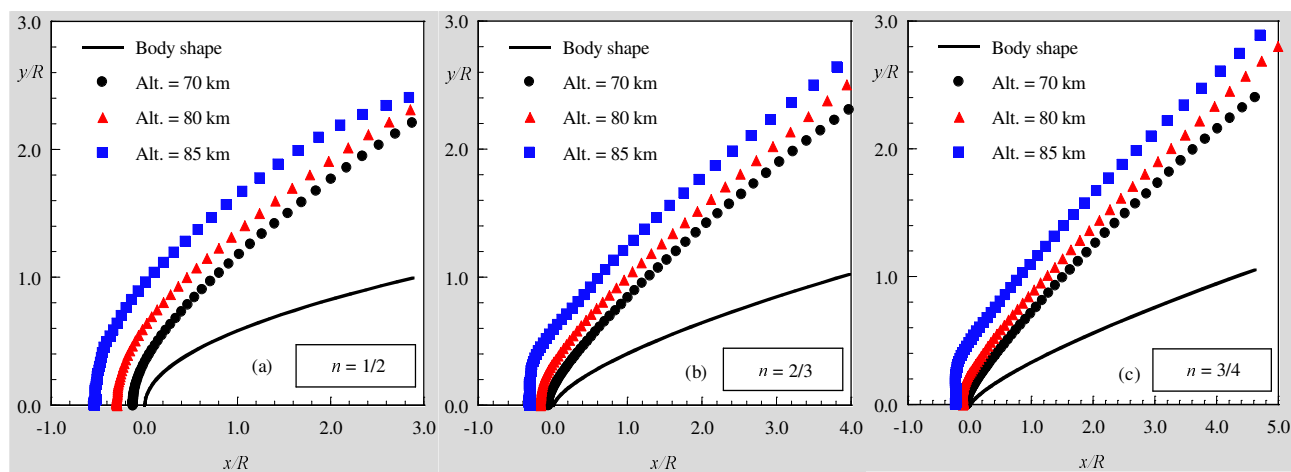


Figure 6: Shock wave shapes on power-law bodies as a function of the altitude for power-law exponent n of (a) $1/2$, (b) $2/3$ and (c) $3/4$.

It was pointed out by Lees and Kubota (1957) that when the freestream Mach number M_∞ is sufficiently large, the hypersonic small-disturbance equations admit similarity solutions for the asymptotic shock wave shapes over power-law bodies ($y \propto x^n$, $0 < n < 1$), where asymptotic refers to the flowfield at large distances downstream of the nose of the body. The hypersonic small-disturbance theory states that, for certain exponent n , a body defined by x^n produces a shock wave of similar shape and profiles of flow properties transverse to the stream direction that are similar at any axial station not too near the nose. At or near the nose, the surface slope, the curvature, and the higher derivatives are infinite, and the similarity solutions break down. In the more general case for $0 < n < 1$, the shock wave grows as x^m . When n grows from zero, m begins by keeping the constant value $m = 2/3$, and if n keeps on growing towards unity, m remains equal to n .

By assuming that power-law bodies generate power-law shock waves in accordance with hypersonic small-disturbance theory, the shock location coordinates shown in Fig. (6) were used to approximate the shape of the shock wave with a curve fit. A fitting algorithm was performed over these points to approximate the shock shape as a power law curve of the following form,

$$y = A(x + B)^m \tag{2}$$

where A is the shock-wave power-law constant, B is the distance from the nose of the leading edge to the shock wave curve fit along the stagnation streamline, and m is the shock-wave power-law exponent.

For comparison purpose, two forms of the curve fit were considered in defining the shock shape: (1) A and B were found by keeping $m = 2/3$ for $n < 2/3$ cases, (2) $m = n$ for $n \geq 2/3$ cases, and (3) A , B and m were found to provide the best curve fit solutions where n and m stand for body and shock wave power-law exponents, respectively.

It is important to mention that the fitting process was performed over the points yielded by DSMC simulations located far from the nose region, say $x/R > 1.0$, where it is expected that the blunt nose effects are not significant. It is also important to recall that the shock wave shape at the vicinity of the nose is not correctly predicted by the theoretical solutions, since the hypersonic slender body approximations are violated close to or at the nose of the leading edges as explained above.

Curve fit solutions for shock shape over the body power-law exponent n of $1/2$ are displayed in Fig. (7a) for altitude of 70 km. In this figure, the solutions given by $m = 2/3$ and $m = 0.670$ represent, respectively, two forms of the curve fit solutions mentioned above. For comparison purpose, the form $m = n = 1/2$ is also displayed in this figure. It is apparent from Fig. (7a) that, except for the form $m = n = 1/2$, the curve fit solutions present a good agreement, by visual inspection, with those solutions provided by the DSMC simulation. Nevertheless, as the maximum absolute error between the DSMC solutions and the curve fit solutions are calculated for coordinate points located at $x/R > 1.0$, it is found that the best fit is obtained for that form of the fitting process where A , B and m were found in order to yield the best solution.

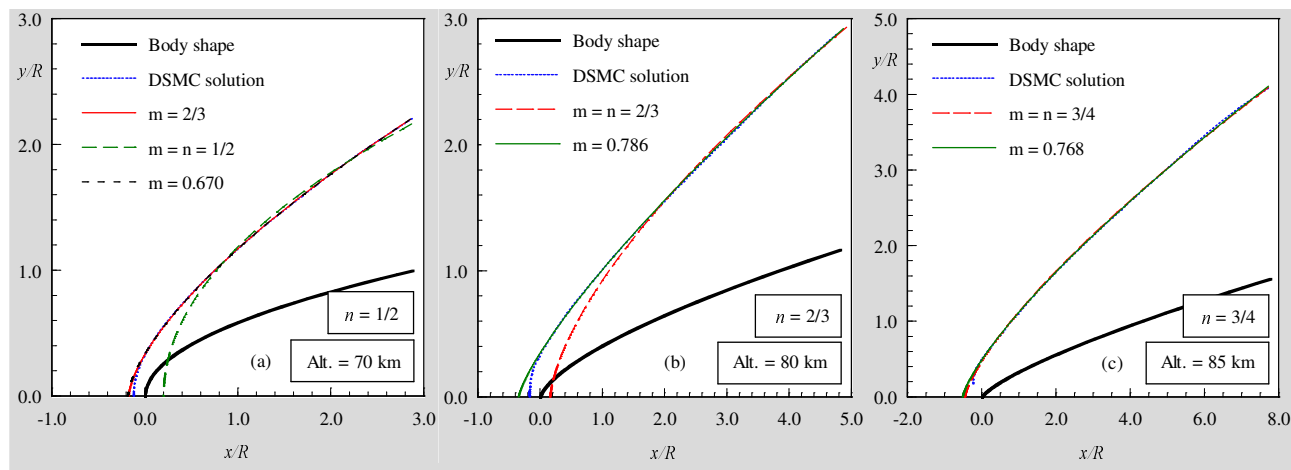


Figure 7: Shock wave shapes on power-law bodies for power-law exponent n of (a) $1/2$ and altitude of 70 km, (b) $2/3$ and altitude of 80 km, and (c) $3/4$ and altitude of 85 km.

Shock shape curve fit solutions for body power-law exponent n of $2/3$ are displayed in Fig. (7b) for altitude of 80 km. The curve fit solutions shown in this set of figures were obtained according to Eq.(2) by two different forms; in the first form, A and B were found by keeping m equal to the body shape, $m = n$; in the second form, A , B and m were found in order to obtain the best fit.

Referring to Fig. (7b), it is noted that the curve fit given by $m = n = 2/3$ present a reasonable agreement far from the nose of the leading edge. Nonetheless, the curve fit solution given by m equal to 0.786 present an excellent agreement with those solutions provided by the DSMC simulation. Once again, the curve-fitted solution deviates from the DSMC solution close to the nose of the leading edge, as would be expected.

Finally, curve fit solutions for shock shape over the body power-law exponent n of $3/4$ are displayed in Fig. (7c) for altitude of 85 km. In this figure, the solutions given by $m = n = 3/4$ and $m = 0.768$ represent, respectively, two forms of the curve fit solutions mentioned above. It is clearly seen in this figure that the curve fit solutions given by present a remarkable agreement with those solutions provided by the DSMC simulation.

According to Figs. (7a), (7b) and (7c), it is observed that, in general, the solutions are in qualitative agreement with the Lees and Kubota (1957) findings in the sense that the shock wave shape would follow the shape of the body for body power law exponent $n > 2/3$.

At this point, it should be emphasized that the curve fit exponents are very sensitive to the number of coordinate points, which define the shock wave, used in the fitting process. In addition, these coordinate points present fluctuations, originated from the DSMC simulations.

8. Concluding Remarks

This study applies the Direct Simulation Monte Carlo method to investigate the shock wave structure for a family of power-law leading edges. The calculations have provided information concerning the nature of the shock wave detachment distance, shock wave thickness and shock wave shape resulting from variations on the power-law exponent and on the freestream Knudsen number for the idealized situation of two-dimensional hypersonic rarefied flow.

The analysis showed that the shock wave structure was affected by changes on the rarefaction via altitude. It was found that the shock wave standoff and the shock wave thickness increased with the altitude rise. In addition, the shock wave was displaced further upstream the nose of the leading edges with increasing the altitude. It was also found that the shock wave standoff distance and the shock wave thickness for the power-law bodies are lower than that for the circular body with the same tangency to a wedge of specified oblique angle. Moreover, the computational results indicated that the shock wave shape grows with power law form ($\propto x^m$), for the power-law bodies investigated.

9. References

- Alexander, F. J., Garcia, A. L., and Alder, B. J., 1998, "Cell Size Dependence of Transport Coefficient in Stochastic Particle Algorithms", *Physics of Fluids*, Vol. 10, No. 6, pp. 1540-1542.
- Alexander, F. J., Garcia, A. L., and Alder, B. J., 2000, "Erratum: Cell Size Dependence of Transport Coefficient is Stochastic Particle Algorithms", *Physics of Fluids*, Vol. 12, No. 3, pp. 731-731.
- Bird, G. A., 1981, "Monte Carlo Simulation in an Engineering Context", *Progress in Astronautics and Aeronautics: Rarefied gas Dynamics*, Ed. Sam S. Fisher, Vol. 74, part I, AIAA New York, pp. 239-255.
- Bird, G. A., 1989, "Perception of Numerical Method in Rarefied Gasdynamics", *Rarefied gas Dynamics: Theoretical and Computational Techniques*, Eds. E. P. Muntz, and D. P. Weaver and D. H. Campbell, Vol. 118, *Progress in Astronautics and Aeronautics*, AIAA, New York, pp. 374-395.
- Bird, G. A., 1994, "Molecular Gas Dynamics and the Direct Simulation of Gas Flows", Oxford University Press, Oxford, England, UK.
- Borgnakke, C. and Larsen, P. S., 1975, "Statistical Collision Model for Monte Carlo Simulation of Polyatomic Gas Mixture", *Journal of computational Physics*, Vol. 18, No. 4, pp. 405-420.
- Garcia, A. L., and Wagner, W., 2000, "Time Step Truncation Error in Direct Simulation Monte Carlo", *Physics of Fluids*, Vol. 12, No. 10, 2000, pp. 2621-2633.
- Guo, K. and Liaw, G.-S., 2001, "A Review: Boundary Conditions for the DSMC Method", *Proceedings of the 35th AIAA Thermophysics Conference*, AIAA Paper 2001-2953, Anaheim, CA, 11-14 June.
- Hadjiconstantinou, N. G., 2000, "Analysis of Discretization in the Direct Simulation Monte Carlo", *Physics of Fluids*, Vol. 12, No. 10, pp. 2634-2638.
- Lees, L. and Kubota, T., 1957, "Inviscid Hypersonic Flow over Blunt-Nosed Slender Bodies", *Journal of Aeronautical Sciences*, Vol. 24, No. 3, pp. 195-202.
- Nonweiler, T. R. F., 1959, "Aerodynamic Problems of Manned Space Vehicles", *Journal of the Royal Aeronautical Society*, Vol. 63, Sept, pp. 521-528.
- Mason, W. H. and Lee, J., 1994, "Aerodynamically Blunt and Sharp Bodies", *Journal of Spacecraft and Rockets*, Vol. 31, No. 3, pp. 378-382.
- Santos, W. F. N. and Lewis, M. J., 2002, "Power Law Shaped Leading Edges in Rarefied Hypersonic Flow", *Journal of Spacecraft and Rockets*, Vol. 39, No. 6, pp. 917-925.
- Santos, W. F. N. and Lewis, M. J., 2005a, "Aerothermodynamic Performance Analysis of Hypersonic Flow on Power Law Leading Edges", *Journal of Spacecraft and Rockets*, Vol. 42, No. 4, pp. 588-597.
- Santos, W. F. N. and Lewis, M. J., 2005b, "Calculation of Shock Wave Structure over Power Law Bodies in Hypersonic Flow", *Journal of Spacecraft and Rockets*, Vol. 42, No. 2, pp. 213-222.
- Van Dyke, M. D., 1954, "A Study of Hypersonic Small-Disturbance Theory", NACA TN-3173.